(Received 3 November 2025, Accepted 26 December 2025, Scheduled 26 January 2026)

Design and Execution of Miniaturized Multi-Band Antenna for Next-Generation Wireless Communication System

Prasanna L. Zade[1,*], Sachin S. Khade[1,*], Deveshree Marotkar[2], Vaishali Dhede[3], Pravin Tajane[1], Pranjali Jumale[4], and Prabhakar Dorge[1]

[1] *Yeshwantrao Chavan College of Engineering, Nagpur, India*
[2] *GHRCEM, Nagpur India*
[3] *Jaihind College of Engineering, Pune, India*
[4] *G.H.Raisoni College of Engineering, Nagpur, India*

ABSTRACT: This paper describes the design methodology of a compact multiband microstrip patch antenna intended for next-generation wireless communication applications. The proposed antenna operates over seven distinct frequency bands: 1.25–1.32 GHz, 2.30–2.44 GHz, 2.50–2.75 GHz, 2.92–3.25 GHz, 3.40–3.65 GHz, 3.70–4.23 GHz, and 4.70–6.0 GHz. These operating bands support a wide range of wireless services, including LTE, 5G communications, Wi-MAX, ISM applications, radar systems, and broadband wireless communications. Multiband performance is achieved through the incorporation of three strategically placed slits in the radiating patch, along with a square split-ring resonator (SSRR). By adjusting the dimensions of the slits and the position of the SSRR, the operating frequency bands can be effectively tuned. The proposed antenna occupies a compact footprint of $40 \times 40\,\text{mm}^2$ and consists of a radiating patch, a partial ground plane, and an SSRR structure. Simulation results demonstrate resonant frequencies at 1.3, 2.38, 2.66, 3.0, 3.5, 4.2, 4.9, and 5.7 GHz. Owing to its compact size, multiband capability, and simple structure, the proposed antenna offers advantages in terms of reduced cost, lower system complexity, and miniaturization, making it suitable for modern wireless communication systems.

1. INTRODUCTION

With the rapid advancement of wireless communication technologies, the demand for mobile devices capable of operating across multiple frequency bands has increased significantly. This trend has created an urgent need for compact antennas that can support next-generation wireless communication systems. The proposed antenna is designed to operate over multiple frequency bands, making it suitable for a wide range of wireless applications, including GSM 1800, Bluetooth, Wi-MAX, Wi-Fi/WLAN, and mid-band 5G communications.

Sub-6 GHz 5G networks offer key advantages such as high data rates, low latency, improved reliability, and the capability to support massive device connectivity. These characteristics are essential for emerging smart technologies in areas such as healthcare, entertainment, smart cities, and smart agriculture [1–3].

Compact microstrip patch antennas are a promising solution for 5G applications due to their low profile, ease of integration, and compatibility with modern communication systems. They can be readily fabricated using photolithography techniques, enabling cost-effective large-scale production. Although conventional patch antennas are limited by narrow bandwidth, recent advancements in materials and antenna design techniques have significantly enhanced bandwidth and radiation performance. As a result, such antennas are increasingly attractive for 5G networks, where wide bandwidth and reliable coverage are critical [4].

The flexibility of compact patch antennas allows their integration onto unconventional and conformal surfaces, thereby expanding deployment opportunities in urban and industrial environments. Several techniques — such as the use of thick substrates, incorporation of slots and slits in the radiating patch, and implementation of partial ground planes loaded with split-ring resonators (SRRs) — have been shown to improve bandwidth and achieve antenna miniaturization, albeit with increased design complexity. The inclusion of resonant structures in the ground plane introduces additional operating bands, leading to a notable enhancement in overall bandwidth. Furthermore, SRRs and other loading techniques enable multiband operation and size reduction [5–6, 10, 11].

This paper presents a detailed analysis of the proposed multiband antenna, supported by simulation results and experimental validation of a fabricated prototype. The antenna employs slits in the radiating patch and an SRR integrated with a partial ground plane to achieve multiband performance. The prototype is fabricated on an FR4 glass-epoxy substrate with compact dimensions of $40\times40\times1.6\,\text{mm}^3$. The proposed antenna successfully covers the frequency bands required for next-generation wireless communication systems while maintaining adequate bandwidth, high radiation efficiency, and stable radiation patterns.

* Corresponding authors: Prasanna L. Zade (zadepl@gmail.com); Sachin S. Khade (sac_mob@rediffmail.com).

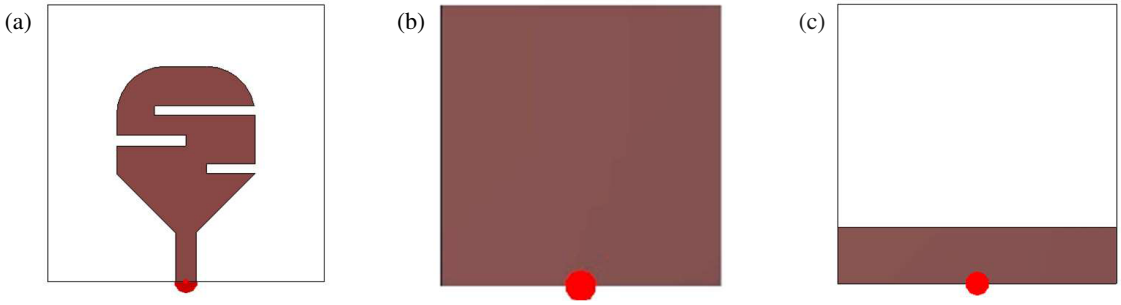

FIGURE 1. (a) Radiating patch. (b) Full GP. (c) Partial G.P.

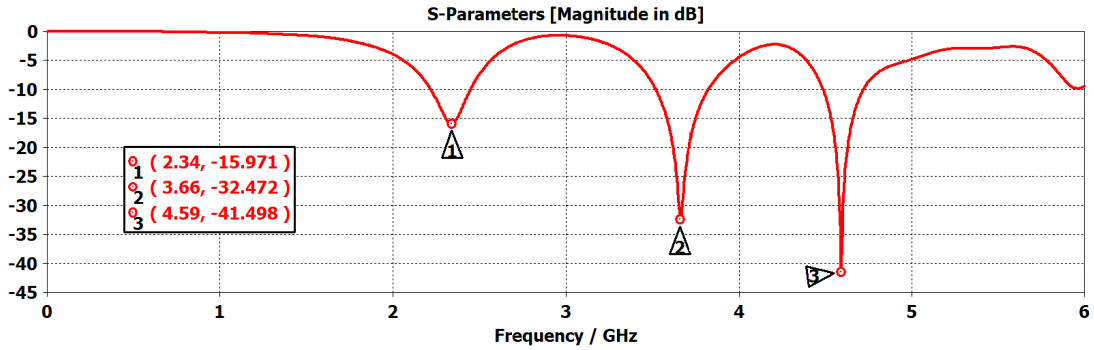

FIGURE 2. S_{11} of proposed (iteration 1) antenna.

2. METHODOLOGY

A novel compact monopole patch antenna featuring three asymmetrically sized slits in the radiating element is presented. The antenna employs a partial ground plane with an integrated square split-ring resonator (SRR) on the reverse side of the substrate. A systematic design and optimization strategy was implemented to achieve high-performance characteristics tailored for next-generation 5G and sub-6 GHz wireless communication applications. The antenna development was conducted through a structured, step-by-step approach, resulting in a 36% reduction in overall antenna size, as detailed in the following sections.

2.1. Antenna Design with Partial Ground Plane

The proposed iteration-1 antenna design process begins with a comparative evaluation of full ground plane (full G.P.) and partial ground plane (partial G.P.) configurations. Conventional patch antennas employing a full ground plane exhibit high capacitance between the feed line and the ground, which adversely affects the resonant behaviour. In contrast, the introduction of a partial ground plane reduces this capacitance, thereby increasing the effective electrical length and shifting the resonant frequency toward lower values. Under this configuration, the patch antenna transitions from behaving as a conventional cavity resonator to functioning as a printed monopole radiator.

Simulation results indicate that the performance obtained with a full ground plane does not meet the desired specifications. By incorporating a partial ground plane, the fringing fields are significantly enhanced, leading to an increase in the effective electrical length and enabling resonance at lower frequencies. This approach facilitates antenna miniaturization without compromising performance [8, 9]. Furthermore, the partial ground plane configuration improves the reflection coefficient and enhances the radiation efficiency of the antenna. The proposed design was simulated, and the corresponding results are presented in Figure 2.

The initial antenna dimensions were $50 \times 50\,\text{mm}^2$, featuring a distinctive geometry resembling a table tennis racket. Antenna size and performance were subsequently optimized through the introduction of three slots in the radiating patch. The optimized antenna configuration is illustrated in Figure 1(a), while Figure 1(b) and Figure 1(c) depict the antenna with a full ground plane and a partial ground plane, respectively. This optimized design supports three resonant frequency bands at 2.34, 3.66, and 4.59 GHz, with corresponding bandwidths of 370, 350, and 310 MHz.

The antenna performance was evaluated using S-parameter analysis to examine its impedance behaviour and confirm effective input impedance matching, thereby ensuring efficient radiation at the desired operating frequencies. The incorporation of slots resulted in notable improvements in both gain and bandwidth. The proposed microstrip patch antenna is intended for the operation in the low- and mid-band frequency ranges.

The first resonant band occurs at 2.34 GHz, exhibiting an S_{11} value of -15.97 dB, which is suitable for applications such as Wi-Fi (2.4 GHz), Bluetooth, and other short-range wireless communication systems. The second resonant band appears at approximately 3.66 GHz, with an S_{11} value of -32.47 dB, making it appropriate for wireless broadband services, fixed

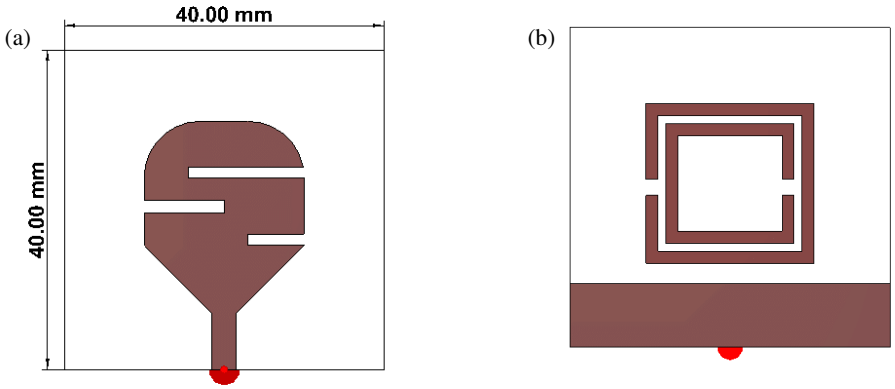

FIGURE 3. (a) Radiating patch. (b) Partial ground plane with SSRR (iteration 2).

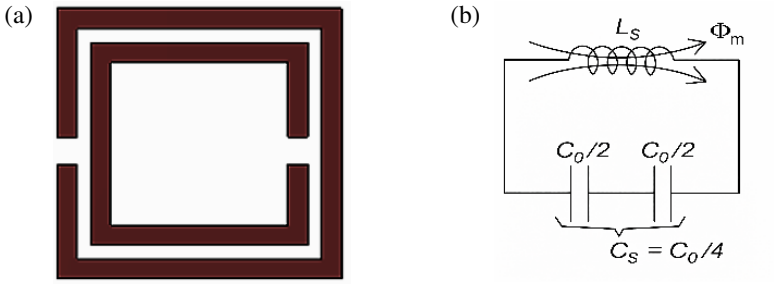

FIGURE 4. (a) R-SRR. (b) Equivalent-circuit models.

wireless access, and selected satellite communication applications within the 3.6–3.8 GHz spectrum. The third resonant band is observed at 4.59 GHz, which is relevant for wireless communication, sensing, and radar applications.

2.2. Size Reduction and Performance Optimization of Antenna

Further optimization of the antenna design resulted in the generation of additional resonant frequency bands, thereby extending its applicability across a wider range of wireless communication systems. This enhancement was achieved by integrating a square split-ring resonator (SSRR) into the ground plane, along with modifying the dimensions of the slits in the radiating patch, specifically by increasing the width of the central slits, as illustrated in Figure 3. The combined use of SSRRs and a partial ground plane on the reverse side of the patch not only contributes to antenna miniaturization but also enables seven distinct resonant frequency bands, substantially broadening the potential application scope of the proposed antenna [8–10].

While earlier studies primarily employed circular split-ring resonators, the proposed iteration-2 antenna design adopts square split-ring resonators to enhance electromagnetic performance. This configuration allows improved control over resonance characteristics and antenna size reduction, while maintaining stable and reliable performance.

Split-ring resonators (SRRs) function as LC resonant circuits when being positioned beneath the radiating patch or in close proximity to the feed region. Their presence increases the effective inductance and slows electromagnetic wave propagation beneath the antenna, thereby extending the effective electrical length. This mechanism enables the antenna to resonate at lower frequencies without increasing its physical dimensions. In addition to shaping the electromagnetic field distribution, the resonator contributes to enhanced overall antenna performance. In microstrip patch antennas, the precise control over the dimensions, spacing, and placement of slots allows the effective fine-tuning of key performance parameters, as well as the modification of radiation characteristics for beam steering and pattern shaping [8, 11, 12].

The SSRR resonance frequency is provided by Equation (1),

$$F = (LsCs)^{-1/2}/2\pi \tag{1}$$

where $Cs = C_0/4$ represents the series capacitance of the upper and lower splits of the R-SRR, respectively,

$$C_0 = 2\pi r_0 C^* \tag{2}$$

where C^* represents the per-unit length capacitance between the rings.

Figure 4 illustrates the square split-ring resonator (SSRR) geometry along with its corresponding equivalent circuit model. The inductance Ls can be approximated by modelling the structure as a single ring and is calculated based on the average radius and width of the resonator. The implementation of a partial ground plane modifies the effective permittivity of the substrate-ground interface, leading to a reduced effective permittivity. This reduction enables a decrease in the physical antenna size while maintaining the same resonant frequency. The primary objective of the proposed patch design is to enhance

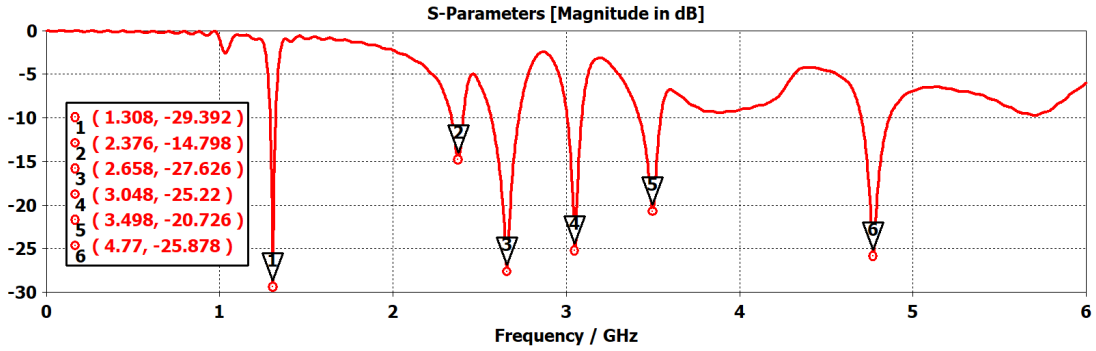

FIGURE 5. Return loss of the proposed antenna .

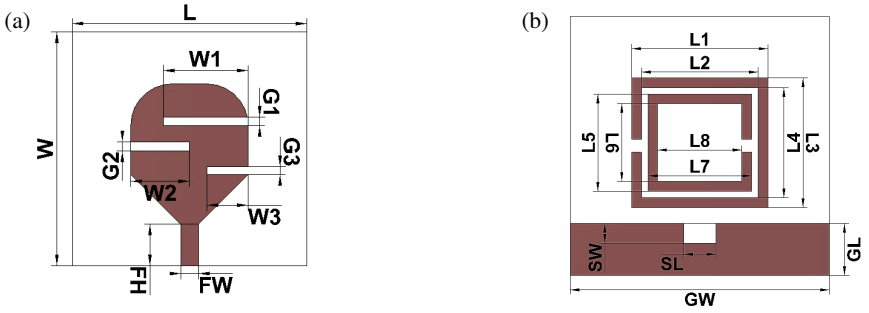

FIGURE 6. (a) Radiating patch view. (b) Ground plane view (iteration 3) with partial ground plane and slit.

antenna performance through optimized multiband operation while achieving size miniaturization [13–16].

Additional resonant bands were generated through the incorporation of ring split-ring resonator (R-SRR) structures, producing resonances at 1.3 GHz (−29.39 dB), 2.37 GHz (−14.78 dB), 2.65 GHz (−27.62 dB), 3.0 GHz (−25.22 dB), 3.49 GHz (−20.72 dB), and 4.77 GHz (−25.87 dB) as shown in Figure 5. These resonant frequencies lie in proximity to several key wireless communication bands, enabling support for applications such as cellular communication within the 2.3–2.4 GHz and 2.5–2.7 GHz ranges, military communication systems, and other specialized radio-frequency platforms. The antenna incorporates a square ring split-ring resonator with an outer dimension of 40 mm, positioned on the ground plane of the dielectric substrate. Owing to its compact configuration, the antenna is well-suited for space-constrained applications, including smartphones, Internet of Things (IoT) devices, and wearable electronics. Square ring resonators are widely employed in microwave components such as filters, antennas, oscillators, and sensors due to their design flexibility. A detailed analysis revealed a noticeable downward shift in resonant frequencies, indicating an effective antenna size reduction of approximately 30%.

Further optimization of the antenna design was achieved by integrating the square split-ring resonator and refining the table tennis racket-shaped patch geometry. Additional frequency bands were obtained by adjusting the depth and width of the three slits on the radiating patch. The optimized antenna exhibits resonances at 1.3, 2.37, 2.65, 3.0, 3.49, 4.77, and 5.8 GHz, with corresponding bandwidths of 120, 145, 160, 145, 160, and 100 MHz. These results confirm the presence of multiple well-defined resonant modes in the S_{11} response, characterized by low return loss, indicating good impedance matching and efficient performance across all operating bands.

The 1.3 GHz band supports L-band satellite communication, as well as military and aviation applications. The widely utilized 2.4 GHz band accommodates Wi-Fi, Bluetooth, ZigBee, and other unlicensed industrial, scientific, and medical (ISM) band applications. The 2.6 GHz band includes 4G LTE Band 7 (2.5–2.69 GHz) and WiMAX services. The 3.0 GHz band is employed in early 5G New Radio (NR) deployments (n77/n78), while the 3.5 GHz band is a core frequency range for 5G NR, particularly band n78 (3.3–3.8 GHz). The 4.77 GHz band supports aeronautical telemetry systems operating in the 4.7–4.8 GHz range and, in certain regions, serves as a mid-band extension for 5G services. The 5.8 GHz band is used for Wi-Fi (IEEE 802.11a/n/ac/ax), electronic toll collection (ETC), and vehicle-to-infrastructure (V2I) communication systems. In addition, the 5.2–5.8 GHz spectrum supports Wi-Fi, WLAN applications, and selected radar systems.

2.3. Inserted Slit in Partial Ground Plane

The introduction of a slit at the center of the partial ground plane beneath the feed line significantly enhances overall antenna performance by improving impedance matching and radiation characteristics, as illustrated in Figure 6 (Iteration 3). This structural modification alters both the capacitive and inductive properties of the antenna due to the redistribution of

TABLE 1. Optimized dimension of the proposed eight-band antenna.

Variable	Dimensions	Variable	Dimensions
W	40 mm	$G1$(Gap 1)	1.4 mm
L	40 mm	$G2$ (Gap 2)	1.6 mm
$W1$	14.38 mm	$G3$ (Gap 3)	1.4 mm
$W2$	10 mm	FH (Feedline Height)	7.0 mm
$W3$	7 mm	FW (Feedline Width)	3 mm
$L1$	21 mm	$L7$ (Length 7)	16 mm
$L2$ (Length 2)	18 mm	$L8$ (Length 8)	13 mm
$L3$ (Length 3)	20 mm	GL (Ground Length)	8 mm
$L4$ (Length 4)	17 mm	GW (Ground Width)	40 mm
$L5$ (Length 5)	15 mm	SW (Slot Width)	5 mm
$L6$ (Length 6)	12 mm	SL (Slot Length)	8 mm

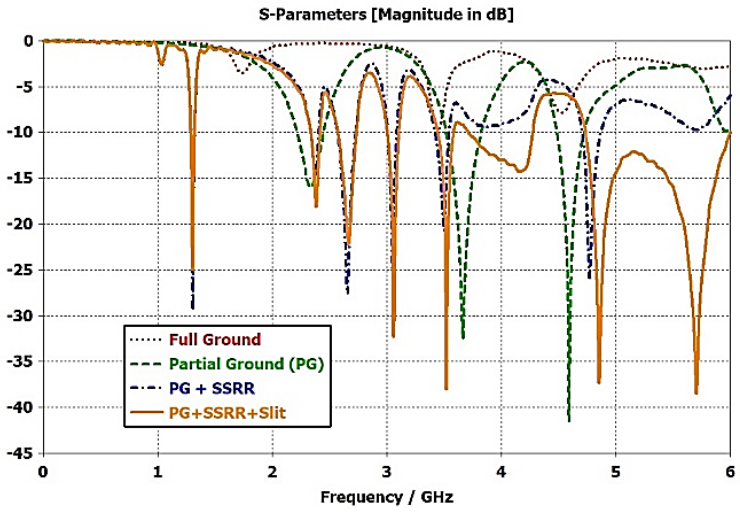

FIGURE 7. Comparative S_{11} with modifications.

surface currents along the slit edges, thereby generating additional resonant frequency bands.

The multiband antenna was meticulously optimized by selecting appropriate parameter values to achieve superior performance, including increased bandwidth, enhanced gain, and reliable multiband operation. These parameters were precisely tuned to ensure efficient radiation and improved impedance matching across the newly introduced target frequency bands. The complete antenna dimensions are summarized in Table 1.

Figure 6(a) illustrates the optimized radiating patch of the racket-shaped antenna, featuring three unequal and asymmetric slits. These slits, positioned along the upper and lower edges of the patch, enable frequency shifts toward both higher and lower bands through careful adjustment of their length and depth [19–21]. Notably, the 2.4 GHz band benefits significantly from improved impedance matching. Additionally, the introduction of a small rectangular slit at the patch center slightly shifts the resonant frequency of the right-hand notch. The antenna employs a microstrip feed line, which extends from the patch and is straightforward to fabricate. Figure 6(b) depicts the ground plane layout, incorporating a square split-ring resonator (SSRR). The inclusion of the SSRR modifies the current distribution on the ground plane, generates additional resonant bands, and enhances impedance matching. Furthermore, it introduces negative permeability and increases the patch's effective inductance, effectively slowing the wave and extending the electrical length without enlarging the physical size. This compact and frequency-selective behaviour makes SSRRs highly suitable for microwave integrated circuits (MICs) and antenna designs [16–18].

Figure 7 presents the S-parameters for four antenna configurations, highlighting the impact of ground plane modifications. The full ground plane exhibits shallow resonances and high reflection, indicating poor impedance matching. Introducing a partial ground plane (PG) produces deeper nulls, exciting additional modes for improved matching. Adding a square split-ring resonator (PG + SSRR) enhances null depth and enables band-selective behaviour, while incorporating a

TABLE 2. Parametric results of antenna.

Frequency GHz	Gain (dBi)	3 dB Angular Beam-Width	Band Width MHz
1.3	2.65	94.2°	70
2.4	2.08	65.6°	140
2.6	2.15	89.5°	250
3.0	3.37	79.6°	330
3.5	2.59	65.23°	250
4.2	3.39	89.20°	350
4.8	3.57	89.20°	530
5.8	4.72	57.8°	1300

central slit (PG + SSRR + slit) achieves the deepest nulls and widest bandwidths across multiple frequencies, demonstrating precise resonance control. By optimizing the central slit depth, eight targeted bands are realized at 1.29, 2.38, 2.6, 3.0, 3.5, 4.2, 4.8, and 5.7 GHz which is shown in Figure 8. Increasing the SSRR spacing reduces capacitance, induces additional resonances, shifts bands upward, and enhances efficiency, while the compact racket-shaped three-slit design minimizes footprint and improves gain. This systematic optimization enables robust multiband operation for next-generation wireless applications.

3. RESULTS AND DISCUSSION

In the first iteration, the proposed antenna was designed and simulated using both full and partial ground planes. This stage achieved resonances at 2.34, 3.66, and 4.59 GHz, with bandwidths of 370, 350, and 310 MHz, respectively, providing performance close to the targeted frequency bands. In Iteration 2, the radiating patch was further optimized by adjusting the depth and width of the side slits, incorporating a partial ground plane, and adding a square split-ring resonator (SSRR). These modifications introduced several additional resonant bands at 1.3, 2.37, 2.65, 3.0, 3.49, 4.77, and 5.8 GHz, with corresponding bandwidths of 120, 145, 160, 145, 160, and 120 MHz. In the final stage (Iteration 3), a central slit was added beneath the feed line on the partial ground plane, creating an eighth resonance while significantly improving impedance matching and enhancing radiation performance, gain, and bandwidth.

The optimization process involved the careful adjustment of the slit design, patch geometry, feed structure, and substrate properties to achieve reliable multiband operation with consistent impedance matching. The antenna exhibits monopole-like behaviour with nearly omnidirectional radiation, as confirmed by 2D polar plots and 3D radiation patterns across all eight resonance frequencies (1.3, 2.4, 2.6, 3.0, 3.5, 4.2, 4.8, and 5.8 GHz) as depicted in Figure 9. Table 2 summarizes the antenna's performance, showing an average gain of 3.3 dBi, with a maximum of 5.11 dBi at 5.8 GHz and a minimum of 2.06 dBi at 2.7 GHz, alongside the associated half-power beamwidths and bandwidths for all targeted frequencies.

Analysing the radiation pattern allows the determination of key parameters, such as gain, directivity, beamwidth, and side lobe levels, providing insight into the antenna's radiation efficiency and the directions of maximum emission. The proposed antenna exhibits monopole-like behaviour, delivering bidirectional radiation in the elevation plane and nearly omnidirectional radiation in the azimuth plane. Conducting a parametric analysis is essential for optimizing patch antenna designs, ensuring stable performance across the targeted frequency bands and confirming the antenna's suitability for next-generation wireless communication applications [22–24].

The surface current distribution on both the radiating patch and ground plane provides critical insight into the antenna's radiation mechanism. Variations in current paths across different frequencies clearly illustrate its multiband operation. Figure 10 depicts the electric surface current vectors on the loaded patch and SSRR across the targeted operating bands. Properly controlled surface currents enhance radiation efficiency, enable precise frequency tuning, and optimize overall performance.

Loading elements influence current flow by introducing localized inductances or capacitances. The addition of slits extends the current path without increasing the physical size of the patch, while the SSRR and partial ground plane redistribute currents, enabling resonance at multiple desired frequencies for compact designs. Narrow slits act as capacitors by creating discontinuities that store electrical energy, whereas longer slots introduce inductance by elongating the current path and adding phase delay. The three patch slits, SSRR, and partial ground plane are strategically positioned to achieve targeted frequency tuning and suppress unwanted surface waves, supporting multiband operation. Currents are strongest along slit edges and regions of high electric field, where edge slots also help suppress sidelobes, enhance beam steering, and modify radiation direction [25, 26]. The antenna exhibits strong surface currents on the radiating patch, indicating good excitation and efficient radiation, as indicated by Table 3.

Radiation efficiency improves significantly with increasing frequency. It is low in the lower bands but rises steadily at higher frequencies, as shown in Figure 11. Small reductions in efficiency in the mid-frequency range suggest localized resonances or structural losses. Overall, the antenna achieves high radiation efficiency of approximately 80–85% above 4 GHz, indicating greater effectiveness at higher frequencies.

The maximum gain monotonically increases with increasing frequency. At lower bands, negative gain values indicate inefficient radiation and energy losses (Figure 12). As frequency

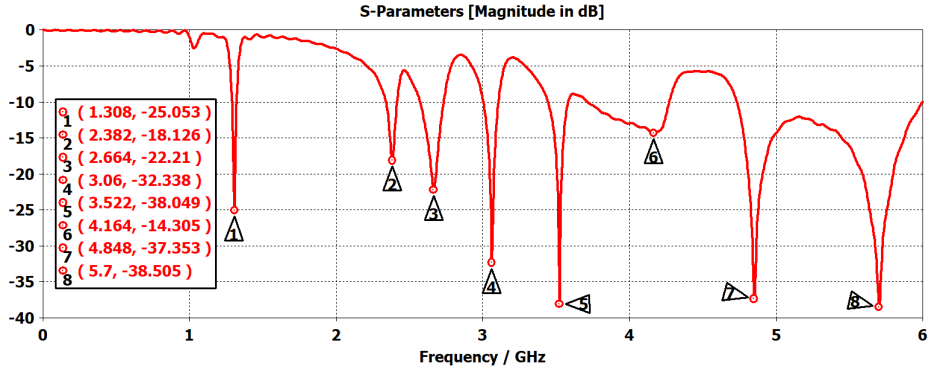

FIGURE 8. Return loss of the proposed antenna.

TABLE 3. Frequency vs surface current results of antenna.

Frequency (GHz)	Surface current A/m	Phase
1.3	107	0 & 157.5
2.38	122.7	292 & 56.25
2.66	99.01	292 & 56.25
3.0	128.2	191 & 56.25
3.5	117.5	270 & 56.25
4.2	61.43	270 & 56.25
4.8	91.85	22.5 & 56.25
5.8	88.92	56.25

TABLE 4. Realize gain to simulated antenna gain.

Frequency GHz	Simulated Gain (dBi)	Realized Gain (dBi)
1.3	2.65	1.32
2.4	2.08	1.5
2.6	2.15	1.2
3.0	3.37	2.67
3.5	2.59	1.69
4.2	3.39	2.59
4.8	3.57	2.73
5.8	4.72	3.56

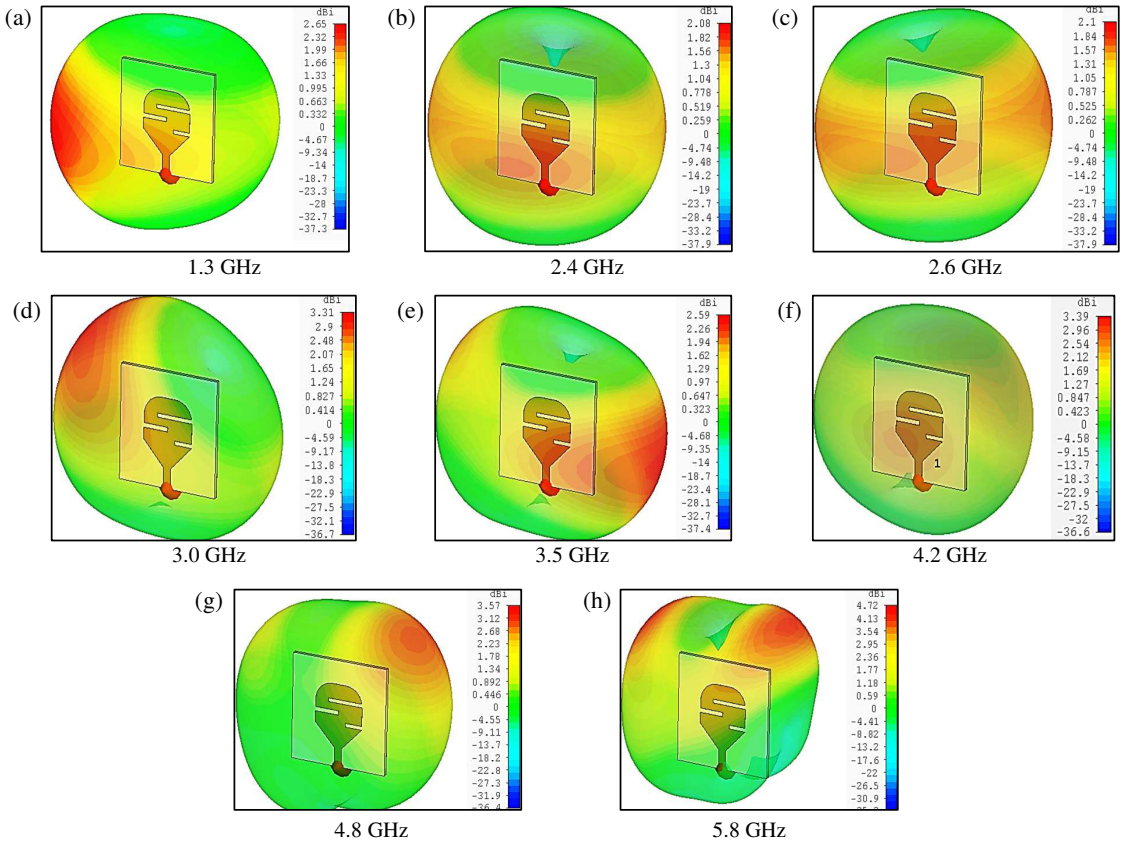

(1)

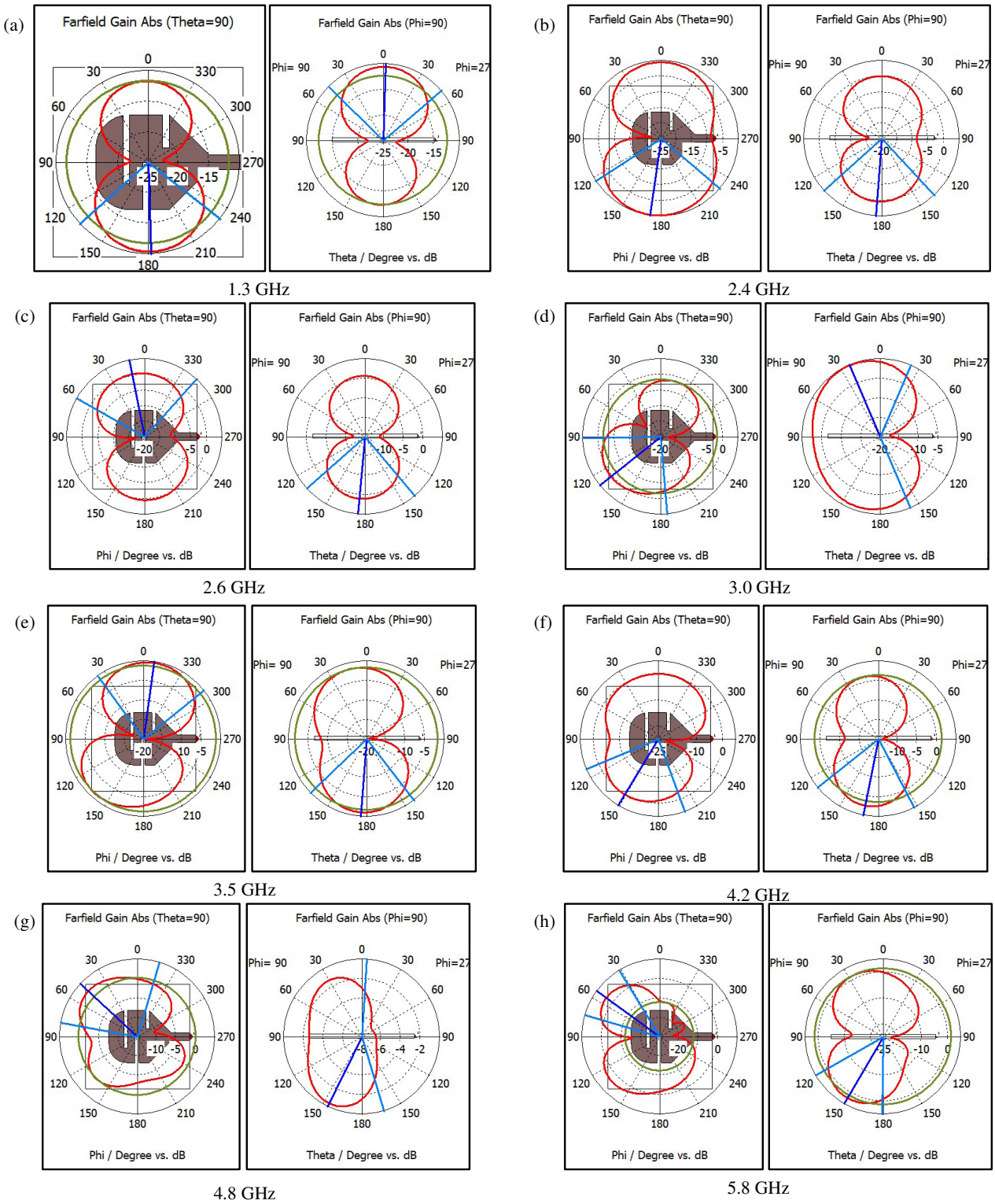

FIGURE 9. (1) — 3D radiation patterns of the antenna at (a) 1.3 GHz, (b) 2.38 GHz, (c) 2.66 GHz, (d) 3.01 GHz, (e) 3.5 GHz, (f) 4.2 GHz, (g) 4.8 GHz and (h) 5.8 GHz. (2) — 2D radiation patterns of the antenna at (a) 1.3 GHz, (b) 2.38 GHz (c) 2.66 GHz, (d) 3.01 GHz, (e) 3.5 GHz, (f) 4.2 GHz, (g) 4.8 GHz, and (h) 5.8 GHz.

rises, the gain becomes positive, reflecting improved radiation efficiency. Minor variations in the mid-band correspond to resonance effects, while the highest gain occurs in the upper frequency bands, confirming superior performance in these regions.

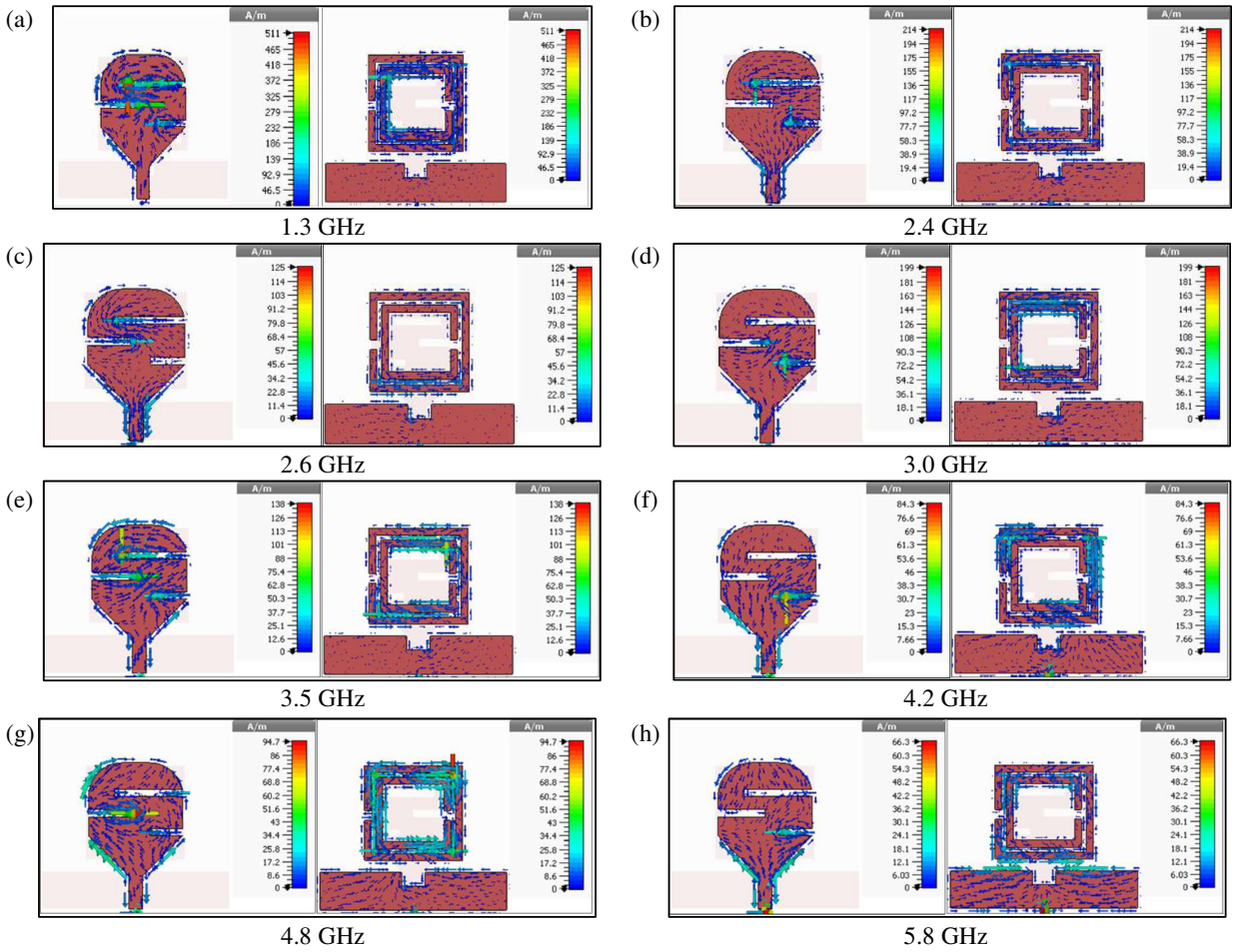

FIGURE 10. The surface current circulation AT. (a) 1.3, (b) 2.4, (c) 2.6, (d) 3.1, (e) 3.5, (f) 4.2, (g) 4.8, and (h) 5.8 GHz.

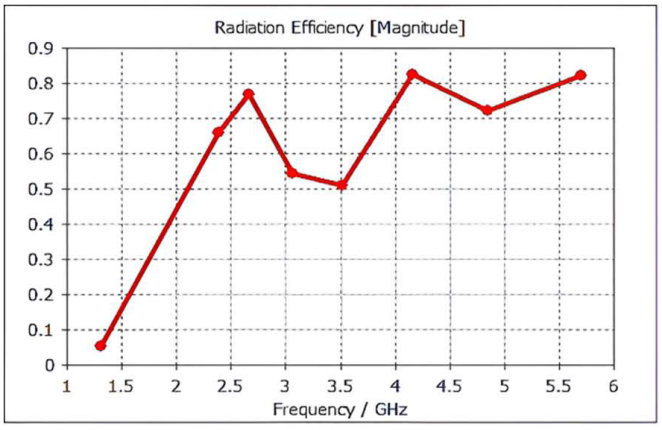

FIGURE 11. Radiation efficiency.

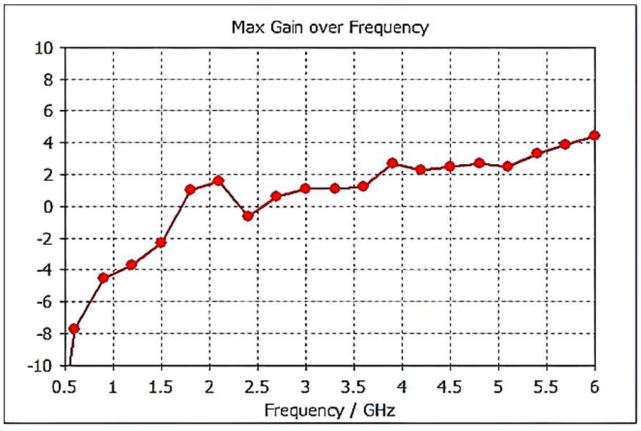

FIGURE 12. Gain vs frequency plot.

4. ANTENNA PROTOTYPE AND IMPLEMENTATION

The fabricated prototype of the proposed antenna is shown in Figure 13, with both front and back views clearly depicted. The miniature multiband patch antenna was fabricated using a milling machine, and its performance was characterized with a Rohde & Schwarz Vector Network Analyzer (ZVH-8).

The main advantage of a multiband antenna is its ability to operate at several desired frequency bands using a single design element. However, this capability introduces additional design and operational complexity, making implementation more challenging compared to single- or dual-band antennas. The prototype is gold-plated, not only for enhanced visualization

TABLE 5. Summary of state-of-the-art literature for implant antenna technology.

Reference No.	Numbers of Band	Resonance Frequency Band GHz	Patch Size mm	Band Width MHz	Gain dB
Proposed antennas	**Multi-band (8)**	**1.3, 2.38, 2.66, 3.0, 3.5, 4.2, 4.8, 5.8**	**40×40×1.6**	**30, 80, 160, 100. 140. 350. 600**	2.65, 2.06, 2.1, 3.71, 2.59, 3.39, 3.57, and 4.72
[5]	Multiband (2)	2.45, 3.6	45×45×1.6	200, 290	>3 dBi
[6]	Multi-band (6)	4.3, 5.0, 6.1, 7.4, 8.9, 9.2	60×55×1.59	68.6, 126.7, 132, 124.3, 191.2, 530.6	1.08, 3.23, 3.36, 2.77, 3.07, 4.87
[7]	Multi-band (6)	2.9, 4.5, 4.9, 5.64	25×16×1.6	200, 972, & 460	2.03, 2.9, 3.02, 3.46
[8]	Multiband (2)	2.45, 2.48	35×29×1.5	256, 304	3.77,4.68
[9]	Multi-band (6)	2.45, 2.53, 3.86, 6.45 6.93, 7.70	47×38×3.18	70, 60, 70, 410 1420	7.31, 8.18, 7.97, 10.6, 5.56, 6.22
[10]	Multi-band (3)	0.86, 1.43, 2.6–6.8	60×60×4	120, 140, 4300	−26, −14, −14.2
[11]	Multi-band (6)	1.25, 1.48, 1.8, 2.25, 2.9	33.7×33.7×1.6	3.2%, 3.4%, 3.33%, 4.5%, 3.1%	1.1, 1.12, 1.15, 1.39, 1.4
[13]	Multi-band (4)	0.45, 1.35, 1.92, 2.57	46.32×25×1.6	185, 151, 77, 218	4.484, 2.59, 3.27, 4.39
[19]	Multi-band (6)	4.3, 5.0, 6.1, 7.4, 8.9, 9.2	60×55×1.59	68.6, 126.7, 132, 124.3, 191.2, 530.6	1.08, 3.23, 3.36, 2.77, 3.07, 4.87
[21]	Multi-band (5)	1.81, 3.6, 4.53, 5.73	70×60×1.6	70, 290, 680, 885	5.71, 5.54, 5.01, 5.32

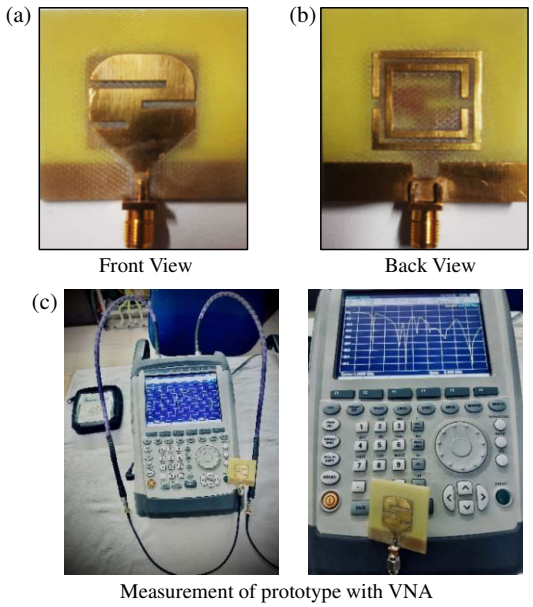

FIGURE 13. Fabrication of the prototype sample.

but also to improve corrosion resistance and extend operational lifespan [27, 28].

5. PERFORMANCE ANALYSIS OF MEASURED VS SIMULATED RESULTS

The simulated antenna parameters were validated through prototype measurements. Figure 14 compares the simulated and measured S-parameters, showing excellent agreement and confirming the accuracy of the design. Frequency tuning for the targeted bands is achieved by adjusting the spacing and width of the SSRR rings, which shifts the resonances to the desired operating frequencies. Likewise, the position, depth, and shape of the three slits on the patch significantly influence multiband operation and overall performance. Specifically, reducing SSRR ring spacing increases the resonant frequency. The plot shows frequency versus return loss, with the red curve representing simulated S_{11} and the blue curve representing measured S_{11}. The close correlation demonstrates good impedance matching and efficient power transfer across the multiband frequencies.

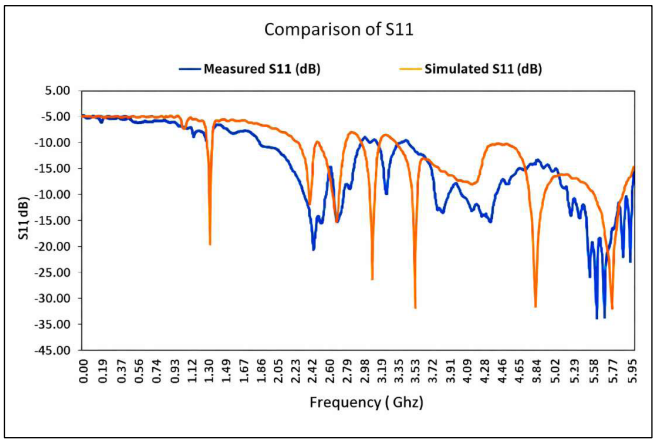

FIGURE 14. Plot for measured vs simulated reflection coefficients $|S_{11}|$ dB values.

Minor fabrication inaccuracies can slightly alter antenna dimensions, causing shifts in resonant frequencies and affecting

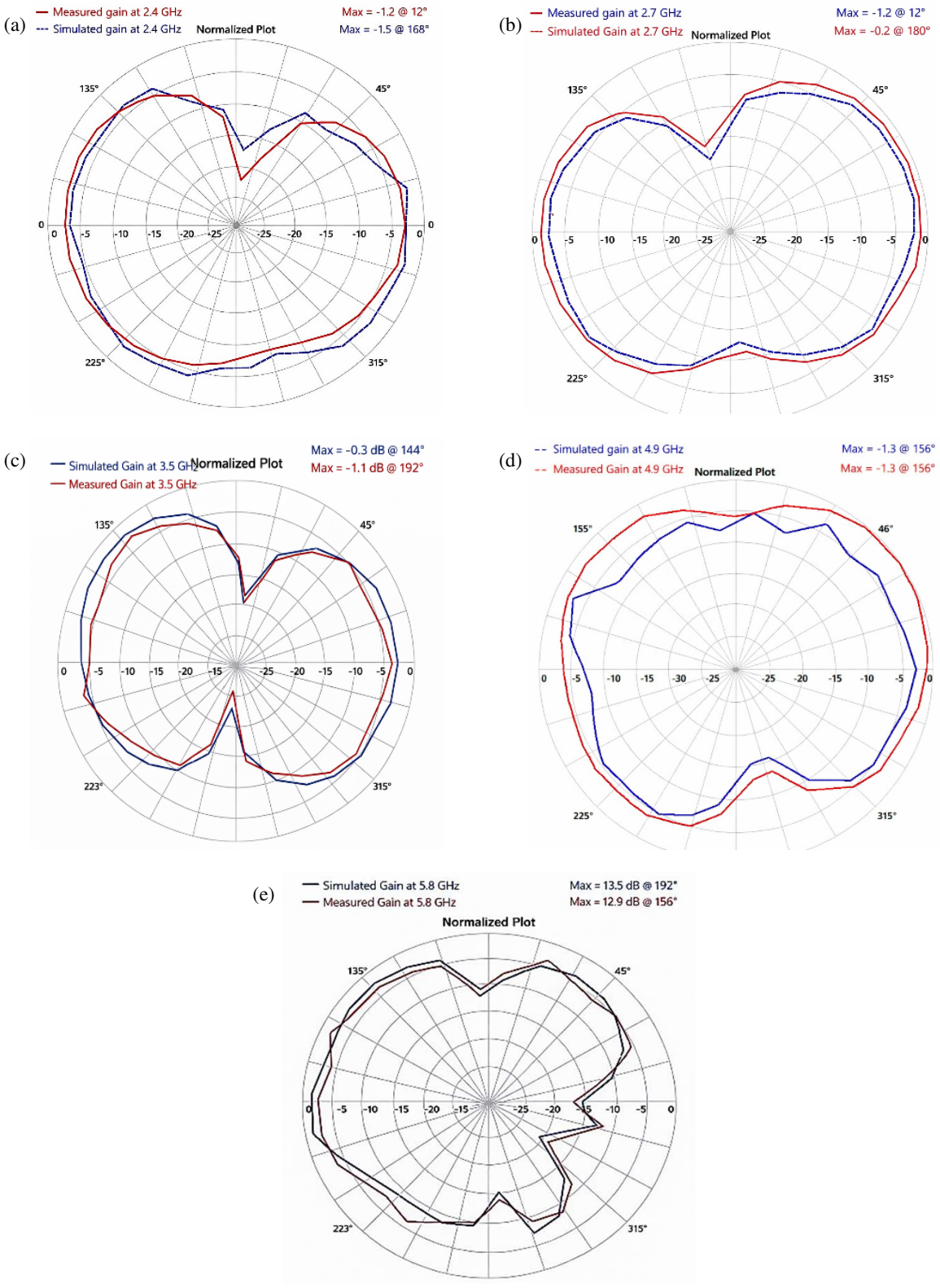

FIGURE 15. Simulated and measured radiation patterns at (a) 2.4 GHz, (b) 2.6 GHz, (c) 3.5 GHz, (d) 4.8 GHz, (e) 5.8 GHz.

impedance matching. Additionally, real substrate properties — such as dielectric constant, loss tangent, and thickness — may differ from those assumed in simulations. Parasitic effects from the SMA connector and soldering, as well as measurement factors like cable losses and connector mismatches, can further influence results. Simulations are typically conducted under ideal conditions, whereas the fabricated antenna operates with a finite ground plane in a real-world environment.

Radiation patterns were measured using an antenna measurement system, and the E-plane patterns were compared with

simulations. Figure 15 presents the measured 2D radiation patterns at the targeted frequencies, showing excellent agreement with simulated gain (red curve for simulated, blue for measured), with both capturing the main radiation lobes characteristic of co-polarized emission. Table 4 compares the realized and simulated gains. The E-field exhibits maximum radiation normal to the antenna, while the H-field forms circular loops around the monopole, producing omnidirectional radiation in the horizontal plane across all targeted frequency bands [29].

6. COMPARISON WITH PREVIOUS STUDIES

A comparative analysis of the proposed antenna with previously reported designs is summarized in Table 5. Although earlier patch antennas demonstrate multiband functionality, they are generally limited by larger physical size, fewer resonant bands, narrower bandwidths, and lower gain. In contrast, the proposed design achieves a compact form factor while supporting a greater number of resonance frequencies with enhanced bandwidth and higher gain, highlighting its superior performance and suitability for next-generation multiband wireless communication applications.

7. CONCLUSION

The proposed antenna features a single patch that operates across eight distinct resonant frequency bands. Compared to conventional designs, this multiband single-patch approach offers several advantages: it reduces the overall size, eliminates the need for multiple antennas for different bands, minimizes hardware complexity, and ensures reliable performance. Such antennas are particularly well-suited for applications in Wi-Fi, Bluetooth, LTE, 5G, and IoT devices, where compactness, low weight, and design integration flexibility are critical. The antenna has been carefully optimized and fabricated using advanced techniques to meet the stringent requirements of 5G communication systems, including low latency, high data rates, and dependable connectivity. It supports resonance at 1.3, 2.38, 2.66, 3.0, 3.5, 4.2, 4.8, and 5.7 GHz, as well as an ultra-wideband (UWB) frequency. Covering the 1.3–5.8 GHz range, the proposed design is suitable for satellite communications, ISM-band wireless devices, LTE/5G mobile networks, fixed wireless access, radar, and high-speed WLAN. This work presents the design and realization of a compact multiband antenna tailored for next-generation wireless communication systems.

ACKNOWLEDGEMENT

Prasanna L. Zade has made key contributions to conceptualization, methodology, supervision, and writing. Sachin S. Khade has made key contributions to data analysis, formatting, and validation. Prabhakar Dorge made key contributions to investigation, resources, and project management. Vaishali Dhede made key contributions to writing and editing. Pranjali Jumale, Deveshree Marotkar, and Pravin Tajane made key contributions to conducting the discussion, finalization of the paper to great extent, and overall writing.

REFERENCES

[1] Balanis, C. A., *Antenna Theory: Analysis and Design*, John Wiley & Sons, 2016.

[2] Kumar, G. and K. P. Ray, *Broadband Microstrip Antennas*, Artech House, 2003.

[3] Garg, R., *Microstrip Antenna Design Handbook*, Artech House, 2001.

[4] Gupta, A., M. Kumari, M. Sharma, M. H. Alsharif, P. Uthansakul, M. Uthansakul, and S. Bansal, "8-port MIMO antenna at 27 GHz for n261 band and exploring for body centric communication," *PLoS ONE*, Vol. 19, No. 6, e0305524, 2024.

[5] Malathy, E. M., I. R. P. Joe, and P. Ajitha, "Miniaturized dual-band metamaterial-loaded antenna for heterogeneous vehicular communication networks," *IETE Journal of Research*, Vol. 69, No. 5, 2436–2445, 2023.

[6] Hakanoglu, B. G., B. Koc, O. Sen, H. Yalduz, and M. Turkmen, "Stub loaded patch antenna and a novel method for miniaturization at sub 6 GHz 5G and Wi-Fi frequencies," *Advances in Electrical & Computer Engineering*, Vol. 21, No. 2, 23–32, 2021.

[7] Baena, J. D., R. Marqués, F. Medina, and J. Martel, "Artificial magnetic metamaterial design by using spiral resonators," *Physical Review B*, Vol. 69, No. 1, 014402, 2004.

[8] Zade, P. L. and S. S. Khade, "Miniaturized novel multi resonance monopole planar antenna with slots, slits, split ring resonator," *Progress In Electromagnetics Research C*, Vol. 145, 75–82, 2024.

[9] Mazen, K., A. Emran, A. S. Shalaby, and A. Yahya, "Design of multi-band microstrip patch antennas for mid-band 5G wireless communication," *International Journal of Advanced Computer Science and Applications(IJACSA)*, Vol. 12, No. 5, 459–469, 2021.

[10] Gupta, A., V. Kumar, S. Bansal, M. H. Alsharif, A. Jahid, and H.-S. Cho, "A miniaturized tri-band implantable antenna for ISM/WMTS/lower UWB/Wi-Fi frequencies," *Sensors*, Vol. 23, No. 15, 6989, 2023.

[11] Aziz, M. A. A., N. Seman, and T. H. Chua, "Microstrip antenna design with partial ground at frequencies above 20 GHz for 5G telecommunication systems," *Indonesian Journal of Electrical Engineering and Computer Science*, Vol. 15, No. 3, 1466–1473, Sep. 2019.

[12] Khade, S. S., D. B. Bhoyar, K. Kotpalliwar, C. V. Bawankar, and M. S. Kimmatkar, "Four element EC slot MIMO antenna for WLAN, Wi-Fi and 5G applications," *Progress In Electromagnetics Research C*, Vol. 139, 147–158, 2024.

[13] Kulkarni, J., C.-Y.-D. Sim, R. Talware, V. Deshpande, A. Chitre, and J. Anguera, "Design and analysis of dual band tapered-fed monopole antenna for 5G and satellite applications," in *2021 IEEE 18th India Council International Conference (INDICON)*, 1–6, Guwahati, India, 2021.

[14] Baena, J. D., J. Bonache, F. Martín, R. M. Sillero, F. Falcone, T. Lopetegi, M. A. G. Laso, J. Garcia-Garcia, I. Gil, M. F. Portillo, and M. Sorolla, "Equivalent-circuit models for split-ring resonators and complementary split-ring resonators coupled to planar transmission lines," *IEEE Transactions on Microwave Theory and Techniques*, Vol. 53, No. 4, 1451–1461, Apr. 2005.

[15] Ullah, S., S. Ahmad, B. A. Khan, F. A. Tahir, and J. A. Flint, "An hp-shape hexa-band antenna for multi-standard wireless communication systems," *Wireless Networks*, Vol. 25, No. 3, 1361–1369, 2019.

[16] Tripathi, S., N. P. Pathak, and M. Parida, "Dual-band dual-beam microstrip patch antenna for intelligent transportation systems application," in *2018 5th IEEE Uttar Pradesh Section Interna-*

tional Conference on Electrical, Electronics and Computer Engineering (UPCON), 1–5, Gorakhpur, India, 2018.

[17] Li, J.-F., C.-X. Mao, D.-L. Wu, L.-H. Ye, and G. Zhang, "A dual-beam wideband filtering patch antenna with absorptive band-edge radiation nulls," *IEEE Transactions on Antennas and Propagation*, Vol. 69, No. 12, 8926–8931, 2021.

[18] Kannadhasan, S. and A. C. Shagar, "Design and analysis of U-Shaped micro strip patch antenna," in *2017 Third International Conference on Advances in Electrical, Electronics, Information, Communication and Bio-Informatics (AEEICB)*, 367–370, Chennai, India, 2017.

[19] Gupta, M. and V. Mathur, "Koch boundary on the square patch microstrip antenna for ultra wideband applications," *Alexandria Engineering Journal*, Vol. 57, No. 3, 2113–2122, Sep. 2018.

[20] Sarkar, D., K. Saurav, and K. V. Srivastava, "Multi-band microstrip-fed slot antenna loaded with split-ring resonator," *Electronics Letters*, Vol. 50, No. 21, 1498–1500, Oct. 2014.

[21] Raval, F., S. Purohit, and Y. P. Kosta, "Dual-band wearable antenna using split ring resonator," *Waves in Random and Complex Media*, Vol. 26, No. 2, 235–242, 2016.

[22] Taheri, M. M. S., A. Abdipour, and G. F. Pedersen, "Compact penta band printed slot antenna for GSM, Bluetooth, WiMAX, 4G LTE, and WLAN applications," in *2017 11th European Conference on Antennas and Propagation (EUCAP)*, 2152–2154, Paris, France, Mar. 2017.

[23] Xu, B., J. Helander, A. Ericsson, Z. Ying, S. He, M. Gustafsson, and D. Sjöberg, "Investigation of planar near-field measurement of millimeter-wave antenna for 5G application," in *2016 International Symposium on Antennas and Propagation (ISAP)*, 600–601, Okinawa, Japan, 2016.

[24] Liu, H., R. Li, Y. Pan, X. Quan, L. Yang, and L. Zheng, "A multi-broadband planar antenna for GSM/UMTS/LTE and WLAN/WiMAX handsets," *IEEE Transactions on Antennas and Propagation*, Vol. 62, No. 5, 2856–2860, May 2014.

[25] Wang, T., Y.-Z. Yin, J. Yang, Y.-L. Zhang, and J.-J. Xie, "Compact triple-band antenna using defected ground structure for WLAN/WiMAX applications," *Progress In Electromagnetics Research Letters*, Vol. 35, 155–164, 2012.

[26] Janning, D. S. and B. A. Munk, "Effects of surface waves on the currents of truncated periodic arrays," *IEEE Transactions on Antennas and Propagation*, Vol. 50, No. 9, 1254–1265, Sep. 2002.

[27] Krishnan, S., P. Sharma, and O. H. Woon, "Antenna radiation pattern considerations for UWB localization," in *2007 IEEE Antennas and Propagation Society International Symposium*, 333–336, Honolulu, HI, USA, 2007.

[28] Chaparala, R., S. Imamvali, S. Tupakula, K. Prakash, S. Bansal, M. M. Ismail, and A. J. A. Al-Gburi, "Spoof surface plasmon polaritons-based feeder for a dielectric rod antenna at microwave frequencies," *Progress In Electromagnetics Research M*, Vol. 129, 23–32, 2024.

[29] Chaparala, R., S. Imamvali, S. Tupakula, K. Prakash, S. Bansal, M. M. Ismail, and A. J. A. Al-Gburi, "Spoof surface plasmon polaritons-based feeder for a dielectric rod antenna at microwave frequencies." *Progress In Electromagnetics Research M*, Vol. 129, 23–32, 2024.